Shock-induced compaction, melting, and entrapment of atmospheric gases in Martian meteorites.

P. Beck, Tristan Ferroir, Philippe Gillet

Shock-induced compaction, melting, and entrapment of atmospheric gases in Martian meteorites

P. Beck,[1,2] T. Ferroir,[1] and P. Gillet[1]

Received 13 September 2006; revised 29 October 2006; accepted 7 November 2006; published 12 January 2007.

[1] The strongest evidence for a Martian origin of the SNC meteorites is the strong correlation between the rare gas abundances and isotopic compositions in shock-induced melt pockets, and those measured for the Martian atmosphere. However, the formation of melt pockets and the entrapment of atmospheric gases remain poorly understood. Here we report the presence in the melt pockets of three Martian meteorites of the hollandite-structured high-pressure polymorph of feldspar. These occurrences set constraints on the continuum pressure (21–25 GPa), the local temperature increase (2000–2500 K) and the energy delivered during shock. We then test a mechanism for melt pocket formation by compaction of pre-existing porous precursors. The model explains the local temperature increase required for melting and the presence of an atmospheric component in pores that were connected with the Martian atmosphere prior to the shock event. **Citation:** Beck, P., T. Ferroir, and P. Gillet (2007), Shock-induced compaction, melting, and entrapment of atmospheric gases in Martian meteorites, *Geophys. Res. Lett.*, *34*, L01203, doi:10.1029/2006GL028141.

1. Introduction

[2] Almost three decades ago, Mars was suggested as the parent body of a small family of meteorites [*McSween et al.*, 1979; *Walker et al.*, 1979; *Wasson and Wetherill*, 1979], the SNC (Shergottites, Nakhlites and Chassignites) or "Martian meteorites". Besides specific petrological and geochemical signatures indicating a large and well-differentiated parent body, a decisive argument for this singular origin was given by *Bogard and Johnson* [1983]: the rare gases composition of glassy areas encountered in the Martian basalt EETA 79001 was similar to that of the Martian lower atmosphere as measured by the Viking probes. A trapped Martian atmospheric component was successively identified in the Zagami meteorite [*Marti et al.*, 1995] and in the ancient cumulate ALH 84001 [*Gilmour et al.*, 1998]. It has been further shown that the atmospheric signature was specifically carried by melt pockets [*Bogard and Johnson*, 1983; *Marti et al.*, 1995; *Walton et al.*, 2006], small areas ($\sim 10^{-5}$–10^{-3} m in diameter) formed at high pressures during the shock event that launched the meteorite and which record a local temperature increase up to 2500 K. The transient shock conditions are well-recorded in these zones by the crystallisation of specific minerals stable at high pressure and high temperature. This is not the case in the bulk rock where the temperature increase by adiabatic compression is limited to a few hundreds of degrees. The shock event, which ejected the meteorites from the Martian near-surface, is likely also responsible for implanting a sample of the contemporary atmosphere. The exact mechanism(s) that generated the melt pockets, and entrapped a substantial volume of Martian atmosphere, remain poorly resolved.

2. Shock Entrapment of Rare Gases: Observations and Experiments

[3] Pioneering experiments on chondritic targets [*Fredriksson et al.*, 1964] initially showed that gases can be implanted in a meteorite upon shock loading. Since then, with the identification of Martian atmospheric component in EETA 79001, several shock experiments have been performed, under controlled atmosphere, in order to reproduce and understand the mechanism responsible for this process [*Bogard et al.*, 1989; *Wiens*, 1988; *Wiens and Pepin*, 1988]. *Wiens and Pepin* [1988] concluded from experiments on basaltic compositions that the atmospheric gases detected in EETA79001 were probably entrapped during a shock event and proposed that *in situ* melting by void collapse could explain the high efficiency of gas entrapment in melt pockets. A major drawback of this scenario was that the shock pressures proposed for melting along the non-porous Hugoniot for basalt were unrealistically high ($\sim$80 GPa) with regard to the shock pressure estimates available at that time for EETA 79001 ($\sim$35–45 GPa) [*McSween and Jarosewich*, 1983]. Further studies on vug-bearing targets revealed that the presence of sharp density contrasts could trigger local melting and then the incorporation of ambient gases at lower pressure [*Wiens*, 1988]. In addition to the work of *Wiens and Pepin* [1988], *Bogard et al.* [1989] demonstrated that an artificially shocked solid sample of basalt showed systematically lower implantation efficiencies in comparison to the corresponding powdered sample, highlighting the effect of porosity. In addition, from their detailed studies of step heating Ar release, the authors reported similarities in the siting of artificially shock-implanted ^{40}Ar and radiogenic ^{40}Ar.

[4] We present an analytical model, which relates the continuum shock pressure, the initial rock porosity, the formation of melt pockets and the entrapment of atmospheric gases in three Martian basalts (Figure 1).

3. Formation of Melt Pockets: Models

[5] Three mechanisms have been proposed to explain the formation of local hot spots (as high as 2500 K) during a

[1] Laboratoire des Sciences de la Terre, CNRS UMR 5570, Ecole Normale Supérieure de Lyon, Lyon, France.
[2] Now at Geophysical Laboratory, Carnegie Institution of Washington, Washington, DC, USA.

0094-8276/07/2006GL028141

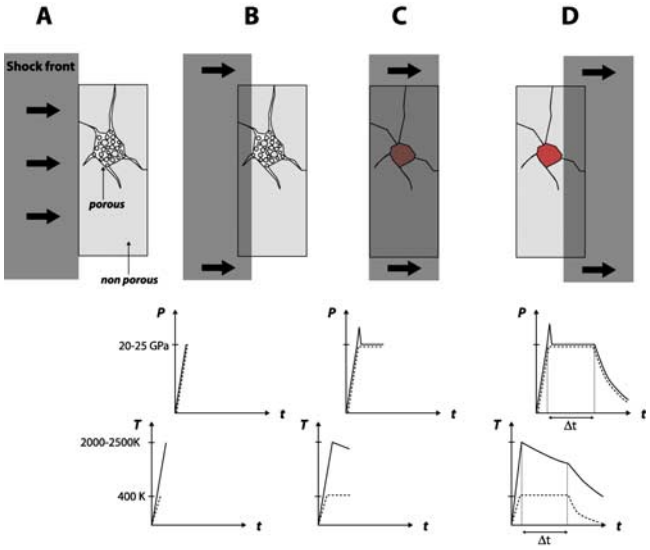

Figure 1. Schematic model for the entrapment of atmospheric gases during a shock event on Martian target rocks. (a) The target rock on Mars is close to the surface and contains porous zones connected to the atmosphere and filled with Martian gases. (b) When the shock front propagates in the non-porous parts of the rock, pressure increases and moderate heating takes place through adiabatic compression (400 K). (c) The passage of the shock front in the porous zone induces collapse of the voids, closure of the cracks connected to the atmosphere, triggers local melting and solubilisation of the atmospheric gases in the melts and crystals formed in the melt pocket. A local pressure spike is associated with pore closure, which duration is short with regard to the continuum shock pressure duration. Then, the continuum shock pressure applies both to porous and non-porous zones (20–25 GPa). The temperature in the compacted porous area (melt pocket) is much higher (2000–2500 K) than that reached in the non-porous parts of the rock (dashed curve). The duration of the shock corresponds to the time during which the pressure and the temperature are constant (Δt). Crystallization of high-pressure minerals like hollandite and stishovite occurs during this time interval within and at the rim of the melt pockets due to the high temperatures. The stability fields of these minerals are used to infer the pressure and temperature conditions reached locally in the melt pockets. (d) When the shock front has passed, pressure drops rapidly, while the temperature decrease is controlled by thermal diffusivity. In order to retain the Martian atmospheric signature in the melt pockets, efficient temperature quench is required to limit the diffusion of the gas species.

shock in a heterogeneous medium. In a first scenario, melt pockets are formed by injection of extraneous molten material. This model was however rejected from the study of melt pocket composition and microtextures [*Walton et al.*, 2005]. The second proposed mechanism is the presence of differences in shock impedance between minerals in a polymineralic rock leading to local reflection and focusing of the wave [*Stöffler et al.*, 1991]. The last mechanism is an extreme case of the previous one, in which a very sharp shock impedance contrast occurs in the rock in the form of voids or pores. This latter scenario, recently modelled by *Heider and Kenkmann* [2003], is likely to produce the highest dissipation of energy.

[6] Shock experiments and Hugoniot data measurements, on a variety of media, also demonstrated that porosity significantly increases the amount of heat transmitted by the shock wave to the target material. Both observational and theoretical studies ascribed this process to a local energy partitioning in the vicinity of the pores [*Campbell et al.*, 1961; *Mader*, 1965]. We explore this model to provide a self consistent picture to Martian atmospheric gases entrapment in melt pockets (Figure 1). We assume that pores connected to the Martian atmosphere were initially present in the rocks before their ejection from Mars. The passage of the shock wave induces the pore collapse, triggers local melting, permits solubilisation at high pressures and temperatures of the atmospheric gases in the melt. Rapid quench of the melt prevents subsequent gas release from the formed glasses and minerals, and their preservation until their analysis on Earth. Porosity can be expected to have occurred subsequently to Martian basalts crystallization, in late stage mineral assemblages, because melt and crystals have different specific volume. Since Martian basalts are surface rocks [*Head et al.*, 2002], one can expect that these pores were connected to Mars surface atmosphere.

[7] The local porosity necessary to induce melting can be evaluated through a model for energy partitioning. The model assumes that the initial shock energy PV/2 (where V is the specific volume) converts into temperature increase and melting enthalpy and is a simplified version of *Ahrens et al.* [1992].

$$\frac{P(V_0 - V)}{2} = F\left(C_p \Delta T + H_m\right) \quad (1)$$

P is the continuum shock pressure, C_p the heat capacity, ΔT the temperature increase, H_m the melting enthalpy, and F the fraction of melted material. V_0 is the specific volume before compaction (porous) and V is the specific volume of the compacted material after the shock (non porous). We assume that, before ejection, Martian basalts contained non-porous and porous areas. The latter were melted during the shock event and produced the melt pockets. If we apply equation (1) locally, to the porous areas, F = 1 since melt pockets are close to complete melting. Porosity, φ, for these areas can thus be defined as:

$$\phi = 1 - \frac{V}{V_0} \Leftrightarrow V_0 = \frac{V}{1 - \phi} \quad (2)$$

Equation (1) can be rewritten:

$$\frac{\phi PV}{2(1-\phi)} = C_p \Delta T + H_m \Leftrightarrow P = 2\frac{(1-\phi)}{\phi}\frac{\left(C_p \Delta T + H_m\right)}{V} \quad (3)$$

From equation (3) the continuum shock pressure required to induce local melting can be inferred as a function of the initial local porosity. Alternatively, if the continuum pressure is known, the porosity required to generate local melting can be determined. The calculation requires only values for H_m and C_p (typically H_m = 350 kJ/kg and C_p =

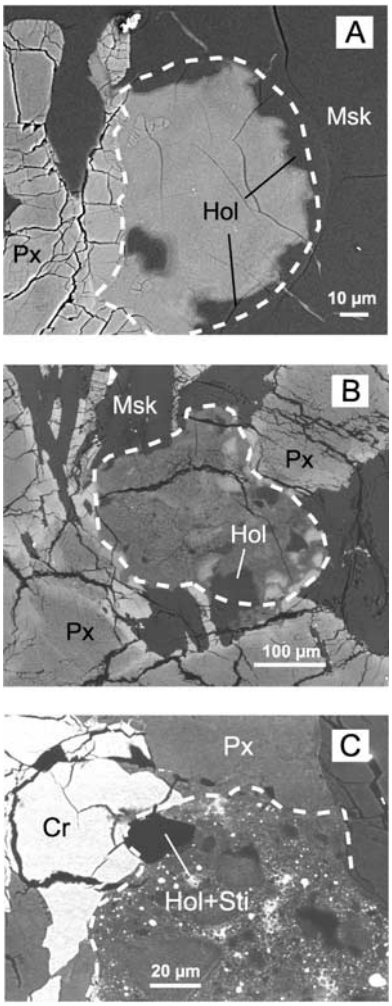

Figure 2. Back-scattered electron images of hollandite grains encountered in the studied meteorites: (a) Zagami, (b) NWA 856 and (c) NWA 480. Images were obtained with a JEOL JSM6301-F scanning electron microscope at SCIAM (Angers).

1400 $J.K^{-1}.kg^{-1}$, the density ($\rho = 1/V = 3000\ kg.m^{-3}$) and the continuum shock P and T (Figure 1). Constraints on the peak shock pressure and temperature can be inferred from the high-pressure mineralogy of the melt pockets.

4. Constraints on the Peak Shock Pressure

[8] Upon shock wave arrival a brief ($\sim$1 μs) pressure spike is expected in the vicinity of the pore with regard to the bulk rock shock pressure [*Heider and Kenkmann*, 2003; *Sharp and DeCarli*, 2006]. Subsequently, pressure homogenizes among the whole rock to its so-called equilibrium shock pressure value, during the shock duration Δt (Figure 1). The continuum pressure developed within the melt veins and melt pockets is hydrostatic and it is constrained to be identical with their surroundings due to stress continuity. The temperature within the melt veins and melt pockets is significantly higher (by up to 2500 K) than in the whole rock, leading to the formation of high-pressure assemblages. Since melt pockets and shock veins mineralogy record similar shock pressures for a same meteorite [*Langenhorst and Poirier*, 2000; *Beck et al.*, 2004], one can suppose that melt pockets high-pressure phases formed during the continuum shock pressure rather than during the initial pressure spike. The continuum pressure can thus be constrained by the known stability fields of these high-pressure minerals.

[9] We have studied by Raman spectroscopy, electron microscopy and electron microprobe the mineralogy of the melt pockets of three Martian basalts. These stones are the Martian basalts Northwest Africa 480 (NWA 480), Northwest Africa 856 (NWA 856) and Zagami [*Barrat et al.*, 2002; *Jambon et al.*, 2002; *McCoy et al.*, 1999]. Hollandite-type feldspar is a common mineral of the shock melt veins and melt pockets of the Martian basalts investigated in this study, and three distinct settings are observed (Figure 2). The first type is encountered at the rims of the melt pockets, where maskelynite, due to heating at high pressures, crystallized and adopted a hollandite structure (Figures 2a and 2b). In some zones it is observed that, as the interior of the melt pocket is approached, hollandite progresses to an assemblage of $(Ca_x,Na_{1-x})Al_{3+x}Si_3O_{11}$ hexaluminosilicates + SiO_2 stishovite [*Beck et al.*, 2004]. The second setting corresponds to isolated rounded grains (with sizes up to 50–60 μm) within the melt pockets. The chemical compositions fall within the albite-anorthite join ((Ca,Na)-hollandite) (Table 1). These two types of hollandite are best explained by solid-state transformations of precursor feldspar grain along the anorthite-albite join. This conclusion is supported by the similar composition of the hollandites with those of magmatic feldspars or maskelynites found far from the melt pockets. The third type of hollandite (Figure 2c), first described by *Langenhorst and Poirier* [2000], is observed in Zagami and NWA 480 in close association with stishovite. The chemical composition of these hollandites falls along the orthoclase-albite join ((K,Na)-hollandite) (Table 1). This association is clearly observed in Zagami, with distinct (K,Na)-hollandite and stishovite grains with crystal textures and habits characteristic of crystallization from a melt. The size of the observed crystal aggregates is 10 μm for each phase. In NWA 480, Raman spectroscopy revealed the superimposition of stishovite and hollandite spectra, though the two phases were not distinguished at the higher magnification of the SEM. Chemical analyses showed that the zone has a composition consistent with a mixture of K-feldspar and SiO_2 (Table 1). The absence of K-feldspar in the melt pocket margin, and it's rare occurrence in the host rock far from the melt pocket [*Barrat et al.*, 2002; *McCoy et al.*, 1999], argues against a solid state transformation of precursor grains to hollandite. A liquidus origin is then favoured.

[10] Early work in the $NaAlSi_3O_8$ system revealed that the hollandite structure is stable for pressure between 20 and 23 GPa at 1000°C [*Liu*, 1978]. However, further studies in the $KAlSi_3O_8$-$NaAlSi_3O_8$ system showed that the solubility of the $NaAlSi_3O_8$ may not exceed 40–50 %, and that this maxima is reached for pressures of the order 22–23 GPa [*Liu*, 2006; *Yagi et al.*, 1994]. Little is known about the stability of the hollandite structure within the $CaAl_2Si_2O_8$-$NaAlSi_3O_8$ system. However, the pressure range, inferred from the maximal Na-hollandite solubility, is in good agreement with the observation of the $(Ca_x,Na_{1-x})Al_{3+x}Si_3O_{11}$ hexa aluminosilicate + SiO_2 stishovite assemblage ($\sim$25 GPa) [*Beck et al.*, 2004]. The observation of the

Table 1. Representative Chemical Compositions of Hollandites Measured in Shergottites[a]

	NWA 480		NWA 856	Zagami	
Oxide	Ca/Na-holl	K/Na-holl+ Sti	Ca/Na-holl	Ca/Na-holl	K/Na-holl
SiO_2	57.76	77.23	56.01	58.32	69.01
TiO_2	0.09	0.46	0.07	0.13	0.03
Al_2O_3	25.02	12.45	27.37	26.11	17.19
Cr_2O_3	0.23	n.d.	0.03	n.d.	n.d.
K_2O	0.65	4.76	0.41	0.48	12.07
Na_2O	5.75	2.48	5.06	5.81	2.03
CaO	9.05	1.10	10.49	9.40	0.38
MgO	0.03	0.01	0.03	0.11	0.01
FeO	0.85	1.69	1.13	0.96	0.56
MnO	0.18	n.d.	n.d.	n.d.	n.d.
Total	99.68	100.37	100.67	101.35	101.383
% Ab	51.4	39.8	52.1	45.9	19.9
% An	44.7	50.4	45.5	51.3	2.1
% Or	3.8	9.8	2.4	2.8	78.0
% Sti		42			

[a]EPMA were obtained using the IFREMER CAMECA SX50 electron microprobe (Brest). Analyses were obtained using mineral and oxide standards at an accelerating voltage of 15 kV, a probe current of 12 nA and a one micron beam diameter. Na was counted first to provide any volatilization during analysis. Repeated microprobe analyses of albite standard show that representative errors are ±0.26% SiO_2, ±0.01 TiO_2, ±0.08 Al_2O_3, ±0.02 FeO, ±0.07 MnO, ±0.01 MgO, ±0.03 CaO, ±0.11 Na_2O, ±0.11 K_2O, ±0.05 Cr_2O_3 in weight.

(K-Na)-hollandite + stishovite assemblage puts additional constraints on P/T shock conditions experienced by the two meteorites NWA 480 and Zagami. In experiments on basaltic compositions [*Wang and Takahashi*, 1999], this association is observed for P > 22.5 GPa and T > 2250 K. This pressure and temperature range is also similar to the P-T conditions at which this assemblage coexists with melt in the $CaAl_2Si_2O_8$-$NaAlSi_3O_8$ system (P = 22 GPa, T = 2450 K) [*Liu*, 2006]. Previous work on Zagami shock veins also reported of this assemblage within shock melt veins [*Langenhorst and Poirier*, 2000]. One can thus remark that both veins and pockets record the same shock pressure.

[11] The pressure recorded by the high-pressure mineralogy of the melt pockets is thus of order 21–25 GPa for all studied meteorites. Constraints on the minimum temperature reached during melt pocket formation can be set using the melting criterion. In the inferred pressure range, the solidus temperature for basalt lies between 2000 and 2500 [*Hirose and Fei*, 2002; *Wang and Takahashi*, 1999].

5. Calculation Results and Conclusion

[12] These pressure and temperature estimates can now be introduced into equation (3); the calculated value for φ is 0.45 ± (0.3). A more sophisticated model, which takes into account the plastic energy dissipated by void collapse [*Meyers et al.*, 1999] leads to a slightly higher value of φ = 0.47 (±0.3). The initial pre-shock porosity of Martian basalts cannot be directly assessed but can be inferred from the actual amount of atmospheric gases solubilised in the melt pockets. *Bogard and Johnson* [1983] measured a 2.10^{-4} m^3 (= 200 mL) volume of Martian atmosphere trapped per kg of glass. Assuming that this volume corresponds to the pore volume present prior to impact melting, a pre-existing local porosity of $\phi = 1 - \frac{V_0}{V} = 1 - \frac{V_0}{2.10^{-4}+V_0} = \sim 0.4$ can be estimated using V = 1/3000 (m^3 kg^{-1}) (Figure 3). This estimate compares well with our calculations from local energetic balance (φ = 0.43–0.5).

[13] Efficient thermal quenching during pressure release is crucial for keeping the Martian atmospheric signature in the melt pockets. If cooling was not rapid enough at the end of the continuum pressure stage, chemical diffusivity of gases with different diffusion coefficients toward the outside of the melt pockets could have erased the strong correlation with the actual Martian atmosphere observed by *Bogard and Johnson* [1983]. In order to model the cooling history of melt pockets, the diffusion equation was solved for temperature. Results show that for melt pocket radii of 100 μm, 500 μm and 1 mm, the cooling times (from T_0 = 2500 to T_f = 500°C) for the whole sphere are 2 ms, 50 ms and 0.2 s respectively, using a typical value of 10^{-6} m^2 s^{-1} for the thermal diffusivity. The cooling time is only marginally modified if one takes into account the latent heat of crystallization of the melt pocket. We can thus conclude that chemical diffusive exchanges were prohibited during melt pocket cooling, which is required to preserve the measured Martian atmospheric signature of the melt pockets.

[14] The proposed model in which local melting occurs by compaction of porosity upon shock wave arrival provides a satisfactory and consistent explanation for the entrapment of a planet's atmosphere in a shocked rock. As previously proposed by *Bogard et al.* [1989], unravelling the way the Martian atmospheric signatures have been implanted in Martian meteorites opens interesting perspectives for inferring the chemical composition of past planetary atmospheres. Dense targets containing porous and non porous areas may provide ideal material of study.

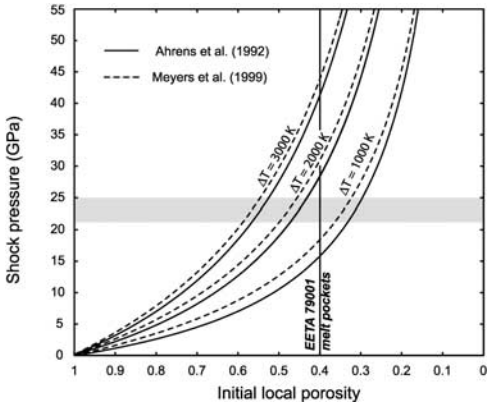

Figure 3. Calculated shock pressure required for local melting as a function of the initial local porosity using *Ahrens et al.* [1992] (solid lines) and *Meyers et al.* [1999] (dashed lines) models. The vertical line corresponds to the volume of atmospheric gases trapped in EETA 79001 glasses converted to pre-existing porosity while the horizontal grey bar is the peak pressure range estimated for the studied meteorites. The density of the compacted basalts is chosen as ρ = 1/V = 3000 $kg.m^{-3}$ and the three sets of curve are drawn corresponding to a temperature increase ΔT of 1000, 2000 and 3000 K. Results show that for the estimated continuum pressure, ~21–25 GPa (grey bar), and for the temperature increase required for melting (2000 K), the calculated value for φ is of ~0.43–0.47 using *Meyers et al.* [1999].

[15] **Acknowledgments.** The technical help from Gilles Montagnac, Marcel Bohn and Maurice Lesourd was greatly appreciated. PB thanks the Region Rhônes Alpes for financial support. This manuscript largely benefited from comments by an anonymous reviewer.

References

Ahrens, T. J., G. M. Bond, W. Yang, and G. Liu (1992), Shock compaction of diamond, in *Shock Waves and High-Strain-Rate Phenomena in Materials*, edited by M. A. Meyer, L. E. Murr, and K. P. Staudhammer, pp. 339–351, CRC Press, Boca Raton, Fla.

Barrat, J. A., P. Gillet, V. Sautter, A. Jambon, M. Javoy, C. Göpel, M. Lesourd, F. Keller, and E. Petit (2002), Petrology and chemistry of the basaltic shergottite North West Africa 480, *Meteorit. Planet. Sci.*, *37*, 487–499.

Beck, P., P. Gillet, L. Gautron, I. Daniel, and A. El Goresy (2004), A new natural high-pressure (Na,Ca)-hexaluminosilicate [$(Ca_xNa_{1-x})Al_{3+x}Si_{3-x}O_{11}$] in shocked Martian meteorites, *Earth Planet. Sci. Lett.*, *219*, 1–12.

Bogard, D. D., and P. Johnson (1983), Martian gases in an Antarctic meteorite?, *Science*, *221*, 651–654.

Bogard, D., F. Hörz, and P. Johnson (1989), Shock-implanted noble gases II: Additional experimental studies and recognition in naturally shocked terrestrial materials, *Meteoritics*, *24*, 113–123.

Campbell, A. W., W. C. Davis, J. B. Ramsay, and J. R. Travis (1961), Shock-initiation of solid explosives, *Phys. Fluids*, *4*, 511–521.

Fredriksson, K., P. S. De Carli, R. O. Pepin, J. H. Reynolds, and G. Turner (1964), Shock emplaced argon in a stony meteorite, *J. Geophys. Res.*, *69*, 1403–1411.

Gilmour, J. D., J. A. Whitby, and G. Turner (1998), Xenon isotopes in irradiated ALH84001: Evidence for shock-induced trapping of ancient Martian atmosphere, *Geochim. Cosmochim. Acta*, *62*, 2555–2571.

Head, J. N., H. J. Melosh, and B. A. Ivanov (2002), Martian meteorite launch: High-speed ejecta from small craters, *Science*, *298*, 1752–1756.

Heider, N., and T. Kenkmann (2003), Numerical simulation of temperature effects at fissures due to shock loading, *Meteorit. Planet. Sci.*, *38*, 1451–1460.

Hirose, K., and Y. Fei (2002), Subsolidus and melting phase relations of basaltic composition in the uppermost lower mantle, *Geochim. Cosmochim. Acta*, *66*, 2099–2108.

Jambon, A., J. A. Barrat, V. Sautter, P. Gillet, C. Göpel, M. Javoy, J. L. Joron, and M. Lesourd (2002), The basaltic shergottite Northwest Africa 856 (NWA 856): Petrology and chemistry, *Meteorit. Planet. Sci.*, *37*, 1147–1164.

Langenhorst, F., and J. P. Poirier (2000), Anatomy of black veins in Zagami: Clues to the formation of high-pressure phase, *Earth Planet. Sci. Lett.*, *184*, 37–55.

Liu, L. G. (1978), High-pressure phase-transformations of albite, jadeite and nepheline, *Earth Planet. Sci. Lett.*, *37*, 438–444.

Liu, X. (2006), Phase relations in the system $KAlSi_3O_8$–$NaAlSi_3O_8$ at high pressure–high temperature conditions and their implication for the petrogenesis of lingunite, *Earth Planet. Sci. Lett.*, *246*, 317–325.

Mader, C. L. (1965), Initiation of detonation by the interactions of shock with density discontinuities, *Phys. Fluids*, *8*, 1811–1816.

Marti, K., J. S. Kim, A. N. Thakur, T. J. McCoy, and K. Keil (1995), Signatures of the Martian atmosphere in glass of the Zagami meteorite, *Science*, *267*, 1981–1984.

McCoy, T. J., M. Wadhwa, and K. Keil (1999), New lithologies in the Zagami meteorite: Evidence for fractional crystallization of a single magma unit on Mars, *Geochim. Cosmochim. Acta*, *63*, 1249–1262.

McSween, H. Y., and E. Jarosewich (1983), Petrogenesis of the Elephant Moraine A79001 meteorite: Multiple magma pulses on the shergottite parent body, *Geochim. Cosmochim. Acta*, *47*, 1501–1513.

McSween, H. Y., E. M. Stolper, L. A. Taylor, R. A. Muntean, G. D. O'Kelley, J. S. Eldridge, S. Biswas, H. T. Ngo, and M. E. Lipschutz (1979), Petrogenetic relationship between Allan Hills 77005 and other achondrites, *Earth Planet. Sci. Lett.*, *45*, 275–284.

Meyers, M. A., D. J. Benton, and E. A. Olevsky (1999), Shock consolidation: Microstructurally-based analysis and computational modelling, *Acta Mater.*, *47*, 2089–2108.

Sharp, T. G., and P. G. DeCarli (2006), Shock effects in meteorites, in *Meteorites and the Early Solar System II*, edited by H. Y. McSween and D. S. Lauretta, pp. 653–677, Univ. of Ariz. Press, Tucson.

Stöffler, D., K. Keil, and E. R. D. Scott (1991), Shock metamorphism of ordinary chondrites, *Geochim. Cosmochim. Acta*, *55*, 3845–3867.

Walker, D., E. M. Stolper, and J. F. Hays (1979), Basaltic volcanism: The importance of planet size, *Proc. Lunar Planet. Sci. Conf.*, *Xth*, 1995–2015.

Walton, E. L., J. G. Spray, and R. Bartoschewitz (2005), A new Martian meteorite from Oman: Mineralogy, petrology, and shock metamorphism of olivine-phyric basaltic shergottite Sayh al Uhaymir 150, *Meteorit. Planet. Sci.*, *40*, 1195–1214.

Walton, E. L., S. P. Keller, and J. G. Spray (2006), Shock implantation of Martian atmospheric argon in four basaltic shergottites: A laser probe $^{40}Ar/^{39}Ar$ investigation, *Geochim. Cosmochim. Acta*, in press.

Wang, W., and E. Takahashi (1999), Subsolidus and melting experiment of a K-rich basaltic composition to 27 GPa: Implication for the behaviour of potassium in the mantle, *Am. Mineral.*, *84*, 357–361.

Wasson, J. T., and G. W. Wetherill (1979), Dynamical chemical and isotopic evidence regarding the formation locations of asteroids and meteorites, in *Asteroids*, pp. 926–974, Univ. of Ariz. Press, Tucson.

Wiens, R. C. (1988), On the sitting of gases shock-emplaced from internal cavities in basalt, *Geochim. Cosmochim. Acta*, *52*, 2775–2783.

Wiens, R. C., and R. O. Pepin (1988), Laboratory shock emplacement of noble gases, nitrogen, and carbon dioxide into basalt, and implications for trapped gases in shergottite EETA 79001, *Geochim. Cosmochim. Acta*, *52*, 295–307.

Yagi, A., T. Suzuki, and M. Akaogi (1994), High-pressure transitions in the system $KAlSi_3O_8$–$NaAlSi_3O_8$, *Phys. Chem. Miner.*, *21*, 12–17.

P. Beck, Geophysical Laboratory, Carnegie Institution of Washington, 5251 Broad Branch Road NW, Washington, DC 20015, USA. (pbeck@ciw.edu)

T. Ferroir and P. Gillet, Laboratoire des Sciences de la Terre, CNRS UMR 5570, Ecole Normale Supérieure de Lyon, 46 allée d'Italie, F-69364 Lyon, France.